

Multi-wavelength pyrometry based on robust statistics and cross-validation of emissivity model

Cite as: Rev. Sci. Instrum. **91**, 114902 (2020); <https://doi.org/10.1063/5.0019847>

Submitted: 25 June 2020 . Accepted: 17 October 2020 . Published Online: 04 November 2020

 Pierre-Yves C. R. Taunay, and Edgar Y. Choueiri



View Online



Export Citation



CrossMark

ARTICLES YOU MAY BE INTERESTED IN

[Two-color, two-dimensional pyrometers based on monochrome and color cameras for high-temperature \(\$> 1000\$ K\) planar measurements](#)



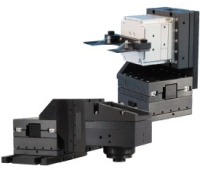
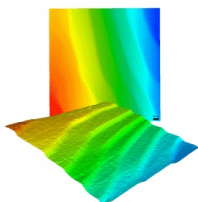
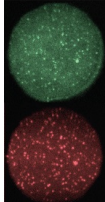
Review of Scientific Instruments **91**, 114901 (2020); <https://doi.org/10.1063/5.0021784>

[Quantitative gas composition analysis method for a wide pressure range up to atmospheric pressure—CO₂ plasma case study](#)

Review of Scientific Instruments **91**, 113501 (2020); <https://doi.org/10.1063/5.0013413>

[Compact integrated optical sensors and electromagnetic actuators for vibration isolation systems in the gravitational-wave detector KAGRA](#)

Review of Scientific Instruments **91**, 115001 (2020); <https://doi.org/10.1063/5.0022242>

 MCL MAD CITY LABS INC. www.madcitylabs.com	<p>Nanopositioning Systems</p> 	<p>Modular Motion Control</p> 	<p>AFM and NSOM Instruments</p> 	<p>Single Molecule Microscopes</p> 
---	--	--	---	--

Multi-wavelength pyrometry based on robust statistics and cross-validation of emissivity model

Cite as: Rev. Sci. Instrum. 91, 114902 (2020); doi: 10.1063/5.0019847

Submitted: 25 June 2020 • Accepted: 17 October 2020 •

Published Online: 4 November 2020



Pierre-Yves C. R. Taunay^{a)}  and Edgar Y. Choueiri

AFFILIATIONS

Electric Propulsion and Plasma Dynamics Laboratory, Princeton University, Princeton, New Jersey 08544, USA

^{a)} Author to whom correspondence should be addressed: ptaunay@princeton.edu

ABSTRACT

A systematic and automated procedure to calculate the temperature of a surface with unknown emissivity from radiance measurements performed at a large number of wavelengths is presented, and statistical methods are applied to quantify its accuracy and precision. Unlike existing multi-wavelength pyrometric approaches, the proposed cross-validated procedure tests multiple emissivity candidates on multiple, randomly chosen subsets of the radiance measurements. The procedure uses solely an emissivity model to provide an accurate temperature value and retrieves the true emissivity from the ratio of the measured radiance to that of a blackbody calculated from the determined temperature. For a given emissivity model, the temperature is computed using the average of all possible combinations of two-wavelength ratios. The emissivity model that minimizes the coefficient of dispersion is selected. Accuracy and precision are quantified for the case of known emissivity. It is shown that, at least in the case where wavelengths are linearly distributed, the method is accurate, the precision increases with the total number of wavelengths, and it is maximized if the ratio of the minimum to maximum wavelength is equal to 2.46. The procedure is applied to both numerical and experimental data from the literature. Excellent agreement of the calculated temperature and emissivity is obtained for both datasets.

Published under license by AIP Publishing. <https://doi.org/10.1063/5.0019847>

I. INTRODUCTION

Pyrometers deduce temperature without contact by first measuring the spectral radiance emitted by a target material at a single or multiple wavelengths. Pyrometry is employed across various industrial and scientific disciplines: its applications include the determination of material temperatures during industrial processes^{1–4} and the evaluation of the temperature of rocket nozzles,⁵ gas turbine blades and combustion chamber,^{6–9} plasma-heated materials,¹⁰ cathodes,^{11–13} and also soot (or other particulates) in engines and furnaces.^{14–16}

The measurement of the thermal spectral radiance is the basis for pyrometry. The temperature is obtained from measured radiance using Planck's law for thermal radiation if the emissivity of the object is known. If the material considered is assumed to have a constant emissivity, such as a gray body or blackbody, a measurement at two different wavelengths yields a temperature calculation, which is independent of the emissivity. In general, however, the emissivity is a function of temperature, material properties, oxidation, and surface condition (e.g., roughness). Its true dependence on

wavelength and temperature is typically unknown and can be time-dependent.

Some approaches compute the temperature without any assumptions about the variation of the emissivity with wavelength.^{5,17–23} Bodrov¹⁷ used a statistical approach in which the most probable temperature of the distribution of two-wavelength temperature predictions is the measured temperature. The author reports errors of 0.1%–2.6% for three objects whose emissivity is a non-monotonic function of wavelength in the range of 1200 K–1300 K. The accurate determination of temperature, however, still requires an emissivity model. Bodrov suggested using the mean temperature to find approximate emissivity values for the start of an iterative procedure. In later uses of this approach, a linear variation of emissivity with wavelength is considered.²⁴

Hagqvist *et al.*^{18,19} proposed an algorithm in which the emissivity is assumed to vary smoothly with wavelength, time, temperature, and surface composition. The method, however, requires an initial, accurate value of the emissivity at the measuring point to be known *a priori*.

References 5 and 20–23 suggest solving a minimization problem where the cost function is the variance of the temperature predictions at multiple wavelengths. The emissivity at each wavelength is an unknown. References 5 and 20–22 assume that the emissivity varies linearly with temperature and propose an iterative algorithm to determine the correct emissivity value. This algorithm still relies on a parameter for which bounds are arbitrarily defined. The method proposed in Ref. 21 cannot be generalized because it is based on a core function that is derived for a *single* temperature. Liang *et al.*²³ derived the initial values for emissivity from a direct least-squares minimization. The authors report good results for multiple hypothetical emissivities and for an experimental case. Unfortunately, using the solution of the least-squares problem as the initial values for the constrained minimization problem means that the temperature variance is already close to optimum (unless the emissivity produced by the least-squares solver is out of bounds). This, in turn, means that the solution of the minimization problem is equal to that of the least-squares one. If the emissivity calculated by the least-squares solver is out of bounds (greater than 1), then the change in the emissivity due to the applied constraints is enough to change the solution.

The knowledge of the functional variation of emissivity with wavelength is required to compute the temperature without any further assumptions or algorithmic restrictions. The literature makes it clear that the model choice for emissivity remains critical to obtain accurate temperature predictions. Typical emissivity models include polynomial or exponential variation with wavelength over a range of interest, though more complicated functional variations exist (see, e.g., Refs. 25–27).

A fully determined system can be formed by performing radiance measurements at N different wavelengths and using an emissivity model that features $N - 1$ unknown coefficients (e.g., a polynomial of order $N - 2$).^{28,29} The unknowns are the $N - 1$ emissivity coefficients and the temperature. The system can then be directly inverted. This solution is attractive because of its simplicity but can introduce large errors when many wavelengths are used due to overfitting of the emissivity²⁸ (although other factors may contribute to the temperature error²⁹). Reference 29 addresses overfitting by applying the method of ridge regression to the determined linear system.

Improved approaches, reviewed in Ref. 30, use a number of wavelengths larger than that of the number of unknown coefficients and a least-squares minimization to solve the over-determined system. The goal is to minimize either the variance of the temperature or the residual (or the chi-squared value) between the predicted and measured radiance.

The minimization of the residual between predicted and measured spectral radiance suffers from multiple problems. Initial values for the parameters should be chosen carefully as convergence is not guaranteed.³¹ A high R-squared value is also not sufficient to guarantee an accurate temperature estimate.^{32–34} Because the parameters of the emissivity cannot be bounded (though the emissivity can), a global optimization algorithm such as simulated annealing cannot be used.

The approach of minimizing the variance of the predicted temperature from two-wavelength ratios does not suffer from the uncertainty in initial emissivity parameters: a multiplicative constant offset in the functional representation of the emissivity disappears

because the emissivity at two different wavelengths appears as a ratio in the temperature calculation. As long as the calculated temperature is accurate, the true emissivity ϵ can be retrieved from the spectral radiance measurements,

$$\epsilon = \frac{I_{\text{measured}}}{I_{\text{bb}}(T_{\text{calculated}})}, \quad (1)$$

where $I_{\text{bb}}(T_{\text{calculated}})$ is the blackbody radiance computed with the predicted temperature $T_{\text{calculated}}$ and I_{measured} is the measured radiance. This approach has been considered with linear^{35–37} or non-linear³⁸ variations of emissivity with wavelength. However, the variance is not a robust measure of statistical dispersion: it is sensitive to outliers in temperature prediction, which can occur when the wavelengths chosen to calculate the temperature are close to one another because the analysis then becomes very sensitive to noise in the radiance measurements.

Both Duvaut *et al.*^{31,34} and Wen *et al.*^{25–27} tested emissivity models for various metals but did not offer a self-contained algorithm to choose which model should be applied to a given surface. Attempts to automate the choice of the emissivity function were performed by Madura *et al.*³⁸ The authors used a three-wavelength pyrometer and chose the most appropriate emissivity function through a multi-step algorithm. However, this algorithm relies on an empirical convergence threshold, which “should be determined experimentally for a given type of pyrometer,” and, therefore, cannot be generalized. Overall, no systematic approach has been developed to choose an acceptable model.

To address the critical issues outlined above, we propose a statistical learning approach for finding the correct emissivity function while maintaining precise and accurate temperature predictions. We optimize the parameters of multiple emissivity models based on a measure of the dispersion of many two-color temperature predictions. The optimization is performed on a given subset of a large number of radiance measurements at different wavelengths (*training* phase). The models are then evaluated concurrently on another smaller subset (*testing* phase). The process is repeated multiple times, and the emissivity model that consistently performs best is chosen.

We present the statistical analysis of the method in Sec. II. The accuracy, precision, and measure of the quality of an emissivity model are demonstrated on simulated numerical data in Sec. II C. We introduce the statistical learning algorithm in Sec. III and present both numerical and experimental results in Sec. IV.

II. STATISTICAL ANALYSIS

Based on N radiance measurements and a given emissivity function, a large number $N_T = \binom{N}{2} = N(N-1)/2$ of two-wavelength temperature predictions can be calculated. We use only two wavelengths because two-term ratio pyrometry is less sensitive to noise compared to ratio pyrometry with three or more wavelengths.³⁹ A statistical analysis of the distribution of temperature predictions gives information about the correctness of the emissivity model chosen and both the accuracy and precision of the temperature prediction.

In this section, we present the method to calculate the two-wavelength temperature predictions and perform a statistical analysis of the generated estimates and their associated error.

A. Temperature calculation

Thermal spectral radiance is the basis for pyrometry. In the range of $T/C_2\lambda \ll 1$, the radiance I at a given wavelength λ and temperature T is given by Wien's approximation,

$$I = \epsilon(\lambda, T) \frac{C_1}{\lambda^5} \exp\left(-\frac{C_2}{T\lambda}\right), \quad (2)$$

where $C_1 = 2hc^2$, $C_2 = hc/k_B$, and ϵ is the emissivity of the material. h , k_B , and c denote Planck's constant, Boltzmann's constant, and the speed of light in vacuum, respectively.

The temperature can be deduced from Eq. (2) if the emissivity is known at every (sampled) wavelength,

$$\hat{T} = \frac{-C_2}{\lambda} \frac{1}{5 \ln \lambda + \ln I - \ln(\epsilon C_1)}. \quad (3)$$

Alternatively, \hat{T} can be calculated from the ratio of radiances $I(\lambda_i)/I(\lambda_j) = I_i/I_j$ at two different wavelengths λ_i and λ_j . For materials with constant emissivity (i.e., blackbody or gray body), the temperature at a single combination of two wavelengths, \hat{T} , is given by

$$\hat{T}(\lambda_i, \lambda_j) = C_2 \frac{1/\lambda_j - 1/\lambda_i}{\ln(I_i/I_j) - 5 \ln(\lambda_j/\lambda_i)}, \quad (4)$$

which allows determining the temperature without knowing the emissivity. In the more general case of an emissivity varying with wavelength, we have

$$\hat{T}(\lambda_i, \lambda_j) = C_2 \frac{1/\lambda_j - 1/\lambda_i}{\ln(I_i/I_j) - 5 \ln(\lambda_j/\lambda_i) - \ln(\epsilon_i/\epsilon_j)}, \quad (5)$$

where $\epsilon_k = \epsilon(\lambda_k)$ is the emissivity at a given wavelength.

We compute an estimate \bar{T} of the true temperature T_0 by averaging Eq. (5) over all wavelength pairs,

$$\bar{T} = \frac{1}{N_T} \sum_{i=1}^{N-1} \sum_{j>i}^N \hat{T}(\lambda_i, \lambda_j). \quad (6)$$

B. Statistical distribution of temperature measurements

We assume in this analysis that normally distributed noise—typical of physical experiments—having a mean of zero and a variance σ_f^2 is present in the signal: $\delta I/I \sim \mathcal{N}(0, \sigma_f^2)$. We consider two cases: (i) repeated measurements of \bar{T} under the same conditions, which give values of \bar{T} and \hat{T} sampled from a distribution to be determined, and (ii) a single measurement of \bar{T} where each two-color prediction \hat{T} represents a sample from an unknown distribution of two-color predictions. The former case is used to quantify the accuracy and precision of the method. The latter is used to derive a criterion to quantify the quality of a chosen emissivity model.

1. Estimation of accuracy and precision

Because of experimental noise (i.e., variation in the radiance I), each pair-wise temperature prediction \hat{T} approximately follows a normal distribution of mean $\mu_{\hat{T}}$ and variance $\sigma_{\hat{T}}^2$,

$$\begin{cases} \mu_{\hat{T}} = T_{\text{eq}}, \\ \sigma_{\hat{T}}^2 = \left(T_{\text{eq}} \frac{\sigma_D}{\mu_D}\right)^2, \end{cases} \quad (7a)$$

$$\begin{cases} \mu_{\hat{T}} = T_{\text{eq}}, \\ \sigma_{\hat{T}}^2 = \left(T_{\text{eq}} \frac{\sigma_D}{\mu_D}\right)^2, \end{cases} \quad (7b)$$

where T_{eq} is the equivalent temperature that would be calculated from the true radiance \bar{I} (i.e., the radiance obtained with the true temperature and emissivity and in the absence of measurement noise),

$$T_{\text{eq}} = \frac{C_2(1/\lambda_j - 1/\lambda_i)}{\ln \bar{I}_i - \ln \bar{I}_j - 5 \ln \lambda_j/\lambda_i - \ln \epsilon_i/\epsilon_j}. \quad (8)$$

The mean μ_D and variance σ_D^2 are those of the denominator of Eq. (5),

$$\begin{cases} \mu_D = \ln \bar{I}_i - \ln \bar{I}_j - 5 \ln \lambda_j/\lambda_i - \ln \epsilon_i/\epsilon_j, \\ \sigma_D^2 = 2\sigma_f^2. \end{cases} \quad (9a)$$

$$\sigma_D^2 = 2\sigma_f^2. \quad (9b)$$

The derivation is shown in the [Appendix](#).

The mean and variance of the scaled error $e_{\hat{T}} = \bar{T}/T_0 - 1$ can be computed from Eqs. (6) and (7),

$$\begin{cases} \mu_{e_{\hat{T}}} = -1 + \frac{1}{T_0 N_T} \sum_{i=1}^{N-1} \sum_{j>i}^N \mu_{\hat{T}}, \\ \sigma_{e_{\hat{T}}}^2 = \frac{1}{(T_0 N_T)^2} \sum_{i=1}^{N-1} \sum_{j>i}^N \sigma_{\hat{T}}^2. \end{cases} \quad (10a)$$

$$\sigma_{e_{\hat{T}}}^2 = \frac{1}{(T_0 N_T)^2} \sum_{i=1}^{N-1} \sum_{j>i}^N \sigma_{\hat{T}}^2. \quad (10b)$$

The accuracy and precision of the method are given by $\mu_{e_{\hat{T}}}$ and $\sigma_{e_{\hat{T}}}$, respectively. When $\mu_{e_{\hat{T}}} \approx 0$, the average temperature \bar{T} is an accurate estimate for the true temperature T_0 .

Filtering effect. A digital filter may reduce the variance of the distribution of the radiance measurements. In the simple case of a moving average filter of window size w , the effect can be quantified. We apply the filter to the *logarithm* of the radiance measurements because it has a smaller variation than the raw radiance measurements. Because the radiance measurements follow a normal distribution [i.e., $I \sim \mathcal{N}(\bar{I}, (\sigma_I \bar{I})^2)$], the filter also modifies the calculation of T_{eq} and μ_D as well as the variance of the average temperature \bar{T} . The calculation of the former two should use the average values of $\ln \bar{I}$, while for the latter the variance is simply rescaled by the window size w ,

$$\begin{cases} \ln \bar{I}_i \rightarrow \frac{1}{w} \sum_{k=i_m}^{i_M} \ln \bar{I}_k, \\ \sigma_{e_{\hat{T}}}^2 \rightarrow \frac{\sigma_{e_{\hat{T}}}^2}{w}, \end{cases} \quad (11a)$$

$$\sigma_{e_{\hat{T}}}^2 \rightarrow \frac{\sigma_{e_{\hat{T}}}^2}{w}, \quad (11b)$$

where $i_m = i - (w - 1)/2$ and $i_M = i + (w - 1)/2$.

Domain of validity. We now seek the conditions under which our approximations are valid. The approximations of the distributions proposed in Sec. II B 1 are valid as long as $\sigma_D/\mu_D \ll 1$. This is not the case if $\mu_D \rightarrow 0$. The expected value of the denominator of \hat{T} , μ_D , finds its minimum for two consecutive wavelengths, λ_i and λ_{i+1} . The radiance at $i + 1$ can be estimated by a Taylor expansion around the point $i + 1$. μ_D then becomes

$$|\mu_D| = \frac{\Delta \lambda}{\lambda_i} \left(\frac{C_2}{T_0 \lambda_i} \right), \quad (12)$$

where $\Delta \lambda$ is the distance between two consecutive wavelengths, and we assumed that the emissivity at the two consecutive wavelengths is constant. In the case of evenly distributed wavelengths,

the wavelength step is

$$\Delta\lambda = \lambda_1 \frac{R}{N-1}, \quad (13)$$

where λ_1 is the base wavelength and $R = \lambda_N/\lambda_1 - 1$ is the wavelength range with λ_N being the largest wavelength considered.

Equation (12) indicates that μ_D is minimum (and, therefore, σ_D/μ_D maximum) for $\lambda_i = \lambda_N$. Using this value of λ_i and the definition of R , the maximum value of N such that $\sigma_D/\mu_D \ll 1$ becomes

$$N_{\text{limit}} \approx 1 + \frac{R}{(1+R)^2} \frac{C_2}{T_0 \lambda_1} \frac{r_{\text{limit}}}{\sigma_D}, \quad (14)$$

where we set σ_D/μ_D to a limit ratio r_{limit} . For a given temperature, minimum wavelength, and σ_D , the largest number of wavelengths that can be used corresponds to $R^* = 1$.

2. Criterion for emissivity model choice

In the ideal case without any measurement noise and with the knowledge of the *exact* emissivity function, the N_T temperature predictions form a degenerate distribution for each sample spectrum measured. When both noise on radiance measurements, $\delta I/I$, and a test emissivity function, $\hat{\epsilon}$, are introduced, the distribution of two-color temperature predictions can take a variety of shapes.

Each two-wavelength temperature calculation is an observation that is drawn individually from a normal distribution. We want to find the distribution that is formed by these observations and quantify the effect of the emissivity error on this particular, unknown, distribution. Bodrov¹⁷ suggested fitting a normal distribution to the two-color temperature predictions. This is correct if the variance of each \hat{T} is the same and the correct emissivity model is chosen. More generally, however, the variance of each \hat{T} is different. The resulting distribution is a *mixture distribution*, f_M , of all of the individual \hat{T} distributions. We illustrate this approach in Fig. 1. Because we use an equal number of two-color temperature samples and individual \hat{T} distributions, the weights that appear in the mixture distribution

are equal,

$$f_M(t) = \frac{1}{N_T} \sum_{i=1}^{N-1} \sum_{j>i}^N f_{\hat{T}}(t), \quad (15)$$

where $f_{\hat{T}}$ is the corresponding distribution of $\hat{T}(\lambda_i, \lambda_j)$. The expected value of this distribution is given by Eq. (6). Each \hat{T} distribution is approximately normal,

$$f_{\hat{T}}(t) \approx \frac{1}{\sqrt{\sigma_{\hat{T}}^2 2\pi}} \exp\left(-\frac{1}{2} \frac{(t - \mu_{\hat{T}})^2}{\sigma_{\hat{T}}^2}\right), \quad (16)$$

where the mean $\mu_{\hat{T}}$ and variance $\sigma_{\hat{T}}^2$ are given by Eq. (7).

a. *Effect of emissivity model on the mixture distribution.* If the correct emissivity model is chosen, we have, by definition, $\mu_{\hat{T}} = T_{\text{eq}} = T_0$. The Taylor expansion of Eq. (15) around T_0 suggests that the distribution f_M can be approximated to the first order by a Cauchy distribution that is centered at T_0 ,

$$f_M(t) \approx f_C(t) = \frac{1}{\pi\gamma} \frac{\gamma^2}{(t - T_0)^2 + \gamma^2}, \quad (17)$$

where γ is given by

$$\gamma = N_T \sqrt{\frac{2}{\pi}} \frac{1}{\sum_{i=1}^{N-1} \sum_{j>i}^N 1/\sigma_{\hat{T}}}. \quad (18)$$

What happens if the wrong emissivity is chosen? By using the definition of the true radiance, the mean and variance, Eq. (7), can be written as

$$\mu_{\hat{T}} = T_{\text{eq}} = T_0(1 + F_{ij})^{-1}, \quad (19a)$$

$$\sigma_{\hat{T}}^2 = \sigma_D^2 \frac{T_0^4}{C_2^2} \left(\frac{\lambda_i \lambda_j}{\lambda_i - \lambda_j} \right)^2 (1 + F_{ij})^{-4}, \quad (19b)$$

where F_{ij} is given by

$$F_{ij} = \frac{T_0}{C_2} \left(\frac{\lambda_i \lambda_j}{\lambda_i - \lambda_j} \right) \ln E_{ij}. \quad (20)$$

The term E_{ij} involves the ratio of the true and estimated emissivities,

$$E_{ij} = \left(\frac{\epsilon_{T,i} \hat{\epsilon}_j}{\epsilon_{T,j} \hat{\epsilon}_i} \right), \quad (21)$$

where ϵ_T is the true emissivity and $\hat{\epsilon}$ is an estimate of the emissivity. The wrong choice of the emissivity model can result in large variations of $\sigma_{\hat{T}}^2$ and of $\mu_{\hat{T}}$ because of the term E_{ij} . This results in a wide mixture distribution function that cannot be well approximated by a narrow Cauchy distribution. As an example, consider the case of a gray body ($\epsilon_{T,i}/\epsilon_{T,j} = 1$) where we assume that the wavelengths are ordered in a strictly increasing fashion ($\forall i, j, \lambda_i < \lambda_j$) and where we consider either a strictly decreasing or increasing test emissivity function, $\hat{\epsilon}$. For a strictly decreasing test function, we have $\forall i, j, E_{ij} < 1 \Rightarrow F_{ij} > 0$. Each individual variance $\sigma_{\hat{T}}^2$ is, therefore, smaller than the one obtained in the ideal case ($E_{ij} = 1 \Leftrightarrow F_{ij} = 0$). This means that each individual normal distribution in Eq. (15) is *narrow*. However, the distribution of individual averages, $\mu_{\hat{T}}$, is now wide and so is the resulting mixture distribution. For a strictly increasing test function, we have $\forall i, j, E_{ij} > 1 \Rightarrow F_{ij} < 0$. Each individual variance $\sigma_{\hat{T}}^2$

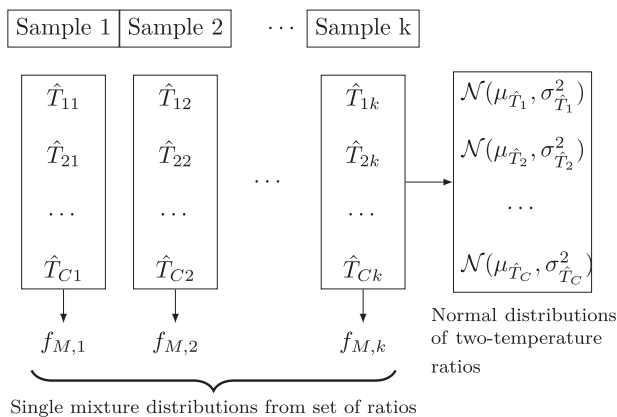


FIG. 1. Illustration of all of the distributions that can be obtained for a set of N wavelengths $\{\lambda_1, \dots, \lambda_N\}$ that form C two-temperature combinations. The sampling is repeated k times.

is, therefore, larger than the one obtained in the ideal case, and we also have a wide distribution of individual averages. We note that the above conclusions do not depend on the ordering of the wavelengths but rather on the sign of the term F_{ij} .

In contrast, the correct choice of the emissivity model results in a narrow peak at the most probable temperature prediction, which is the best estimate of the true temperature T_0 . This suggests that the quality of the chosen emissivity model is related to the width of the Cauchy distribution.

b. Estimate of the dispersion. Multiple methods exist to estimate the dispersion of a distribution. The standard deviation and coefficient of variation are not robust to outliers, which may occur, for example, when the two wavelengths in Eq. (8) are close to each other. Integer moments of a Cauchy distribution (and, therefore, the standard deviation) are also undefined. Robust estimates for the dispersion of a distribution include the coefficient of median absolute deviation or the interquartile range. However, those coefficients have the same unit as the random variable, and it is preferable to perform comparisons between distributions with unitless quantities. To estimate the dispersion in the resulting non-normal distributions, we use the *quartile coefficient of dispersion*, q_d (or *coefficient of quartile variation*), as suggested by Bonett.⁴⁰ It is defined as

$$q_d = \frac{Q_3 - Q_1}{Q_3 + Q_1}, \quad (22)$$

where Q_i is the i th quartile.

In practice, the value of T_0 is unknown, which means that both the mean and variance of each \hat{T} cannot be computed and that, therefore, both the mixture and the Cauchy distributions cannot be directly estimated. An alternative method to estimate the shape of the distributions is necessary. Kernel Density Estimation (KDE) estimates the true distribution of a vector of observations without *a priori* knowledge of the underlying parameters of the distribution. For N samples $\{X_1, \dots, X_N\}$ that are sampled from a given distribution f , the shape of the distribution, \hat{f} , is given by

$$\hat{f}(X) = \frac{1}{Nh} \sum_{k=1}^N K\left(\frac{X - X_k}{h}\right), \quad (23)$$

where K is a positive kernel function and h is a kernel parameter (the “bandwidth”). We use KDE with a Gaussian kernel and an optimal bandwidth found with a grid search to compute the true distribution of the two-color temperature predictions. The Gaussian kernel is

$$K_G(t) = \frac{1}{\sqrt{2\pi}} \exp\left(-\frac{1}{2}t^2\right). \quad (24)$$

The parameters of the Cauchy distribution are found using the maximum likelihood method.

c. Influence of outliers. When a small wavelength separation is used to compute the two-color temperature predictions, noise can result in large deviations (outliers) from the true temperature T_0 . We have observed outliers that are both multiple orders of magnitude higher than the true temperature and also negative. They can have detrimental effects on the accurate computation of the average temperature. To remove outliers in a given sample of two-color predictions, we use a Tukey fence on the Cauchy-like distribution prior to computing the average temperature: predictions outside of the

range of $[Q_1 - \delta \text{IQR}, Q_3 + \delta \text{IQR}]$ are discarded, where δ is a factor to be determined and depends on the distribution chosen to represent the two-color predictions and IQR is the interquartile range. The average temperature that is obtained by this process is also called the *trimmed mean* because we discard part of the distribution to compute it. We note that this is a similar process to computing the coefficient of dispersion as this coefficient is based on the interquartile range, which is also a *trimmed estimator* of the range.

The distribution of a single sample of two-color predictions approximately follows a Cauchy distribution centered at T_0 and with parameter γ . The first and third quartiles are given by $Q_1 = T_0 - \gamma$ and $Q_3 = T_0 + \gamma$, respectively. The interquartile range is, therefore, $\text{IQR} = 2\gamma$. The probability of finding the temperature between two bounds, $T_a = Q_1 - \delta \text{IQR}$ and $T_b = Q_3 + \delta \text{IQR}$, is given by the direct integration of the probability density function [Eq. (17)],

$$\begin{aligned} \mathbb{P}[T_a \leq T \leq T_b] &= \int_{T_a}^{T_b} f_C(s) ds \\ &= \frac{2}{\pi} \arctan(2\delta + 1). \end{aligned} \quad (25)$$

To exclude outliers that represent 1% of the distribution, the corresponding value of δ is

$$\delta_{99} = \frac{1}{2} \left(\tan\left(0.99 \frac{\pi}{2}\right) - 1 \right) \approx 31.3. \quad (26)$$

Note that the large value of δ is the result of the two-color temperature predictions following a Cauchy distribution. A similar calculation for a normal distribution shows that $\delta_{99, \text{normal}} = 1.41$.

Because the value of δ used for the Cauchy distribution is much larger than that of a normal distribution for the same probability, we assume that the resulting normal distributions of \hat{T} and individual \hat{T} are not modified by the fencing operation. For $\delta = 31.3$, the probability of finding a measurement between the bounds T_a and T_b is $\mathbb{P}_{\text{normal}}[T_a \leq T \leq T_b] \approx 1$. Consequently, accuracy and precision, as given by Eq. (10), remain unaffected by the process of removing outliers.

d. Non-uniqueness of best emissivity model. Consider the ideal case of a gray body ($\forall i, j, \epsilon_{T,i} = \epsilon_{T,j} = \epsilon_T$) without any noise ($\sigma_i = 0 \Rightarrow \sigma_{\hat{T}} = 0$). If the test emissivity chosen is also a constant, $\hat{\epsilon}_C$, then each individual \hat{T} is equal to the true temperature, T_0 . However, because we use two-wavelength ratios, the test emissivity does not have to be equal to the true emissivity and may differ by a multiplicative constant.

More generally, we cannot mathematically guarantee that the emissivity model that minimizes the dispersion is unique. The goal of the procedure is to find parameters θ_e for a test emissivity model $\hat{\epsilon}$ such that the mixture distribution features a narrow peak and, therefore, such that all of the two-wavelength emissivity ratios are equal to the corresponding true emissivity ratios (i.e., $E_{ij} = 1$). The corresponding non-linear equation is

$$\mathcal{F}(\lambda_i, \lambda_j, \theta_e) = \frac{\epsilon_{T,i}}{\epsilon_{T,j}}, \quad (27)$$

where \mathcal{F} is a function that represents a test emissivity ratio, which may take any functional form. Because Eq. (27) is non-linear and because the total number of parameters is lower than that of the

number of equations, there cannot be any uniqueness guarantee for the “best” emissivity model.

In practice, the true emissivity is unknown and Eq. (27) is not formally solved. Rather, the true emissivity is retrieved from Eq. (1).

C. Numerical results

We now apply the approximations from Sec. II B to illustrative cases. We investigate the effect of measurement noise on temperature error and demonstrate that the criterion derived for evaluating a chosen emissivity model is sensitive to a proposed emissivity function. In all cases, we make the assumption that $\sigma_I \ll 1$ (low noise measurements).

We treat here the case where wavelengths are separated by a constant offset, which is typical of multi-color pyrometers,

$$\lambda_i = \lambda_1 \left(1 + (i-1) \frac{R}{N-1} \right), \quad (28a)$$

$$\lambda_j = \lambda_1 \left(1 + (j-1) \frac{R}{N-1} \right). \quad (28b)$$

In this case, we obtain closed-form solutions for the accuracy and precision.

1. Effect of measurement noise on temperature error

We assume here that the correct emissivity model has been chosen and numerically evaluate the accuracy and precision of the method subject to measurement noise. Because T_{eq} features the true radiance in its denominator, the temperature ratio T_{eq}/T_0 is close to 1, and therefore, $\mu_D \approx C_2(1/\lambda_j - 1/\lambda_i)/T_0$. The mean value of the scaled error, μ_{e_T} , reduces to zero, which indicates that the average of the two-color predictions is an accurate estimate of the true temperature. Using Eq. (10b), the variance $\sigma_{e_T}^2$ is expressed as

$$\sigma_{e_T}^2 = \frac{8\sigma_I^2}{w} \left(\frac{T_0\lambda_1}{C_2} \right)^2 S, \quad (29)$$

where S is given by

$$S = \frac{1}{N^2 R^2} \sum_{i=1}^{N-1} \sum_{j>i}^N \left(\frac{\left(1 + \frac{(i-1)R}{N-1} \right) \left(1 + \frac{(j-1)R}{N-1} \right)}{i-j} \right)^2. \quad (30)$$

We now compute the precision in the case where (i) the total number of wavelengths is increased and (ii) the range of wavelengths is varied.

a. Asymptotic behavior for a large number of wavelengths. The asymptotic expansion of S as $N \rightarrow +\infty$ is

$$S \sim \frac{\pi^2}{6NR^2} \left(1 + 2R + 2R^2 + R^3 + \frac{1}{5}R^4 \right). \quad (31)$$

The asymptotic error is shown in Fig. 2 as a function of R for $N \geq 10$. The approximation incurs at most an error of 45%. The error drops rapidly as N increases and increases slightly as R increases. Using Eqs. (29) and (31), the variance becomes

$$\sigma_{e_T}^2 \approx \frac{4\pi^2}{3} \frac{\sigma_I^2}{w} \left(\frac{T_0\lambda_1}{C_2} \right)^2 \frac{1}{NR^2} \times \left(1 + 2R + 2R^2 + R^3 + \frac{1}{5}R^4 \right). \quad (32)$$

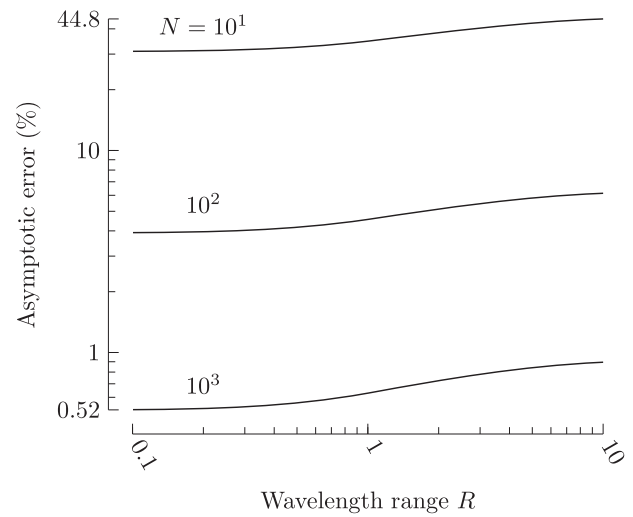


FIG. 2. Error incurred by asymptotic expansion as $N \rightarrow +\infty$.

This indicates that (i) increasing the number of wavelengths will decrease the variance and, therefore, increase the precision and (ii) there exists an optimum value R^* of R for which the variance is minimized and, therefore, the precision is maximized. A simple analysis reveals that $R^* = 1.45987$.

b. General case. For two-color pyrometers ($N = 2$), the variance decreases continuously with the range [$S \sim (1+R)^2/R^2$], which suggests that the largest wavelength separation should be used to maximize precision. For a larger number of wavelengths, the range that maximizes precision is shown in Fig. 3.

Both effects of the total number of wavelengths and the wavelength range are visualized with a contour representation of S in Fig. 4. The optimum R for $N \geq 3$ is also shown as a curve joining the minima in Fig. 4. For a given range, increasing the total

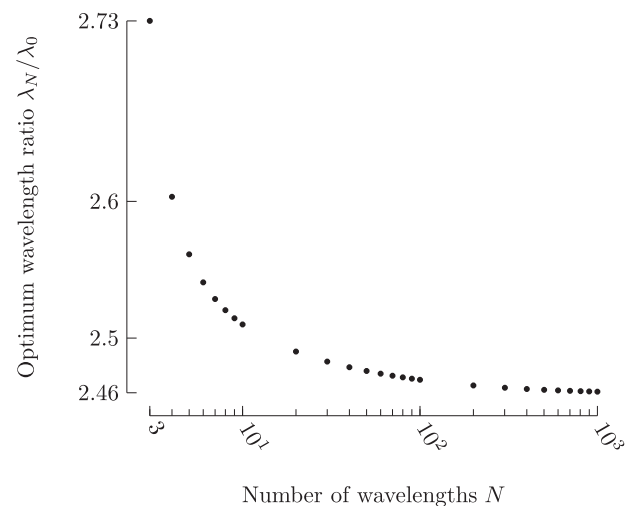


FIG. 3. Optimum wavelength ratio as a function of the total number of wavelengths.

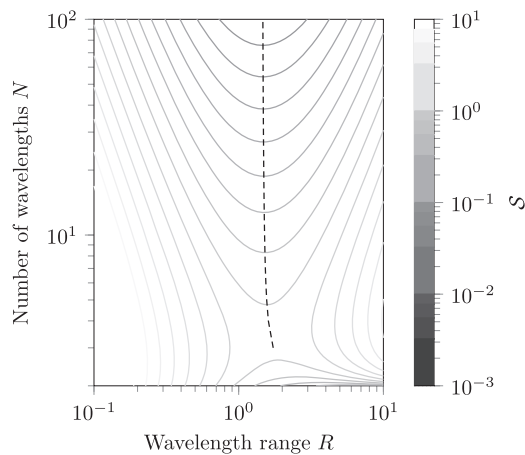


FIG. 4. Contour plot of S . The dashed line indicates the optimum R for $N > 3$.

number of wavelengths decreases the sum S and, therefore, increases the precision.

Figure 5 shows the standard deviation σ_{e_T} and absolute value of the mean μ_{e_T} as a function of the total number of wavelengths considered, for various values of $C_2/(T_0\lambda_1)$, two noise levels ($\sigma_I = 0.01$ and 0.1), and no moving average filter. We use the optimum wavelength range ($R = 1.46$). The quantities are computed using either a Monte Carlo simulation with 10 000 samples (scatter plot) or the approximation from Eq. (10) (dashed and solid lines). The maximum N as derived from Eq. (14) is also shown for a value of r_{limit} of 0.5 as a vertical line. Good agreement is obtained with the variance approximation from Eq. (10) until the maximum N is reached. The mean as computed from the Monte Carlo simulation is not exactly zero, as suggested by our earlier approximation. Its value, however, is small (less than 1% for 10% experimental error), which still suggests that the average of the two-color predictions is a good estimate for the true temperature *under the assumption that the correct emissivity model is chosen*. The Monte Carlo simulations indicate that for a given R increasing the total number of wavelengths results in increasing both the accuracy and the precision (both $|\mu_{e_T}|$ and $\sigma_{e_T}^2$ decrease).

2. Effect of error in the choice of the emissivity model

We now turn our attention to the effect of an incorrect proposed emissivity model. For simplicity, we use a gray body emissivity of 0.5 as our true emissivity. The true radiance is computed with the constant emissivity and a temperature of 3000 K between the wavelengths of 300 nm and 738 nm ($R = 1.46$). We discretize this domain with 50 wavelengths and consider a standard deviation of $\sigma_I = 0.1$ for the simulated normal experimental noise (10% experimental error with 95% confidence) and a moving average filter with a window size of 21. We then apply the test polynomial emissivity,

$$\hat{e}(\lambda) = \sum_{n=0}^{N_e} a_n \lambda^n, \quad (33)$$

where N_e is the order of the polynomial.

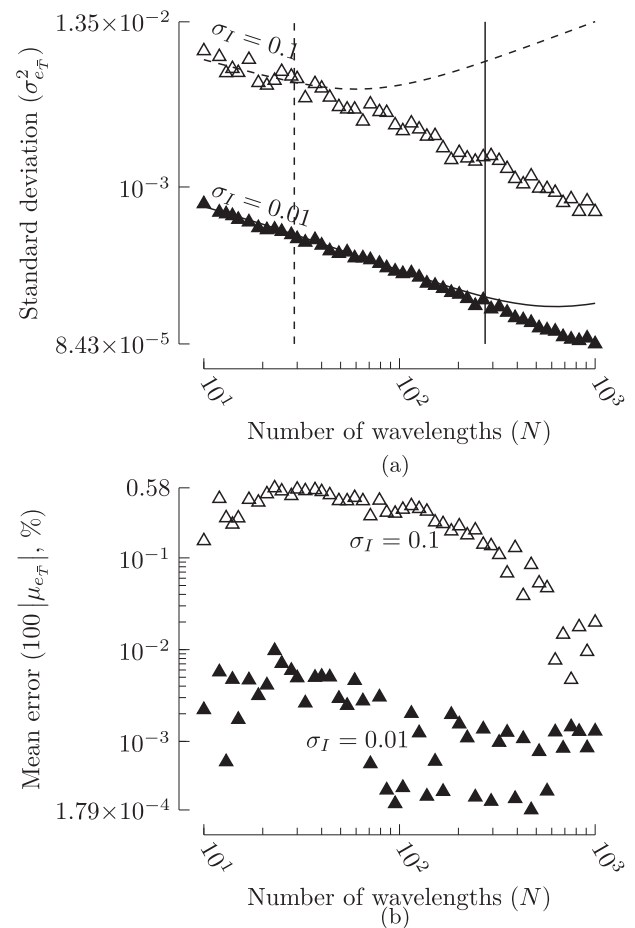


FIG. 5. Effect of the total number of wavelengths on (a) standard deviation (σ_{e_T}) and (b) mean error (μ_{e_T}). Results are obtained through Monte Carlo simulations for two different values of experimental noise. Vertical lines in (a) indicate the maximum number of wavelengths for which the assumptions used to derive mean and standard deviation are valid.

Figure 6 shows the effect of the test emissivity on the distribution of a single sample of two-color predictions, \hat{T} , for four linear test models and the correct one. The distributions were estimated using kernel density estimation (KDE). The KDE uses a Gaussian variable kernel with a bandwidth chosen with a grid-search k -fold cross-validation (5 folds). The KDE, grid-search, and cross-validation are implemented using the `scikit-learn`⁴¹ library. For an incorrect emissivity model, we observe a large dispersion in the distribution function. The correct emissivity model features the smallest dispersion and is centered at the true temperature of 3000 K. Similar results are obtained for higher-order emissivity functions.

The error incurred in calculating the true temperature is shown as a function of quartile dispersion in Fig. 7. Each point is generated by averaging the results of the procedure to calculate \hat{T} , the two-color predictions \hat{T} , and the associated error and quartile dispersion for 1000 artificially generated test spectra. We use a first- or second-order polynomial for the test emissivity. When the functional representation of the emissivity is close to the true emissivity

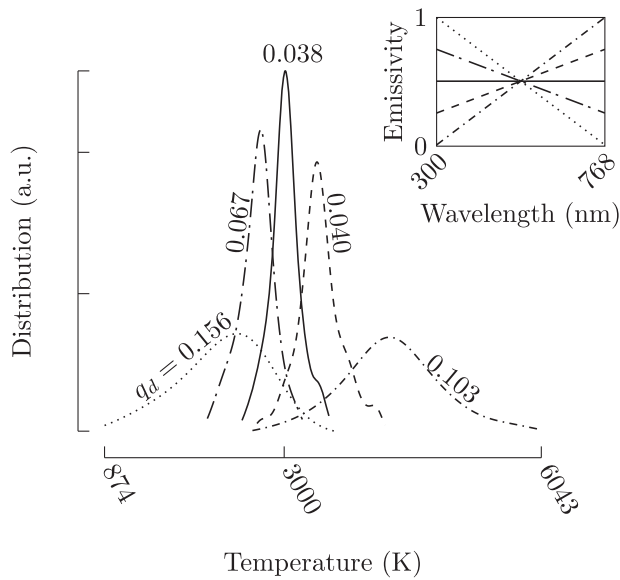


FIG. 6. Distribution of two-color temperature predictions for different first-order emissivity models and the resulting quartile dispersion value, q_d [Eq. (22)]. Inset: corresponding emissivity model.

(i.e., zero slope for the linear emissivity model and zero curvature for the quadratic emissivity model),

- the linear emissivity model has the lowest error that is within 1% of the case of the lowest dispersion;
- the quadratic emissivity model has the lowest dispersion and has an error that is within 0.001% of the case of the lowest error.

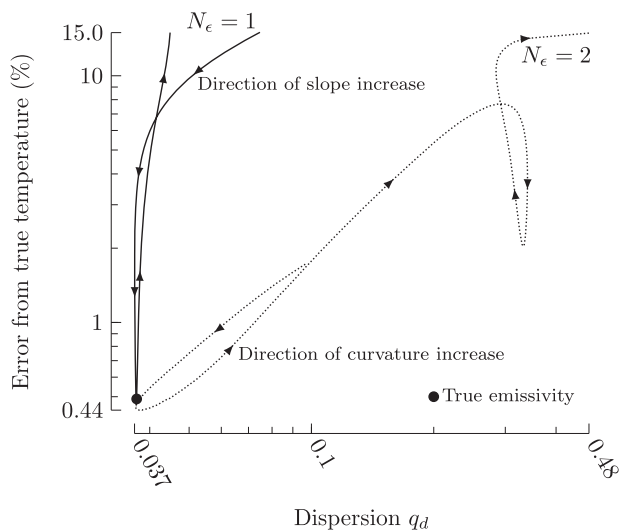


FIG. 7. Error as a function of dispersion for multiple test emissivity functions modeled with a polynomial of order 1 or 2.

The cases with the lowest dispersion also have the smallest variation of emissivity with wavelength. The corresponding estimate of the emissivity is, therefore, close to the true emissivity, which is a constant. In all cases, a low dispersion indicates that the emissivity model is close to the true emissivity. The trade-off between dispersion and error is similar to the bias-variance trade-off.

For multi-color pyrometry measurements that rely on the average of two-color temperatures, we suggest the use of dispersion as an indicator of the quality of the chosen emissivity model. We note that we have applied this method to the entire spectrum available. A cross-validation method with training and testing datasets that are subsets of the entire spectrum available and that use this dispersion measure should allow selecting the correct emissivity function. We describe such an approach in Sec. III.

III. STATISTICAL LEARNING ALGORITHM

We present here a systematic approach to find the best emissivity model such that the temperature is accurately and precisely calculated. We have shown that the quartile coefficient of dispersion q_d [Eq. (22)] is sensitive to the quality of the proposed emissivity model. Minimizing this quantity gives a test emissivity $\hat{\epsilon}$ that yields the correct temperature. We, therefore, set our cost function to be the quartile coefficient of dispersion.

To ensure that the calculated temperature is both accurate and precise, a cross-validation method is necessary. There may, indeed, be instances where a given emissivity model has the lowest dispersion when fitted on the entire dataset while at the same time has a higher error than the optimal model, which is obtained by a cross-validation method. Unlike previous approaches (e.g., least-squares minimization), we do not choose all N wavelengths to “train” each model without validation. Rather, we use the following k -fold methodology to cross-validate each emissivity model and select the most appropriate one.

A. k -fold method

The dataset of wavelengths and radiance measurements of size N is split into two subsets:

- A subset of the data of size N_{train} that is used to calculate the unknown coefficients of each emissivity model such that the cost function is minimized.
- A different subset of the data of size $N_{\text{test}} < N_{\text{train}}$ that calculates the cost function for each optimized model.

We use the Nelder–Mead method,⁴² as implemented in SciPy,⁴³ for the optimization of a proposed model on the training dataset. For computational efficiency, if both N_{train} and N_{test} are large (e.g., 1000 wavelengths or more), the measurements are “binned” into $N_{b,\text{train}}$ and $N_{b,\text{test}}$ ensembles (bins of length L_{bin}), respectively. The median wavelength of each bin is then used for calculations.

The training and testing datasets do not have to be contiguous: the choice of the wavelengths is randomized. The procedure is performed k times (typically 5–10 times) and yields $k - 1$ training and 1 testing fold(s), respectively [i.e., subsets that include a

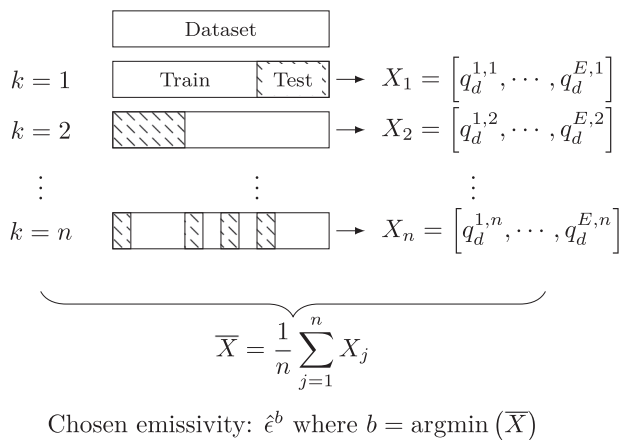


FIG. 8. Schematic of the k -fold method applied to the choice of the emissivity model. Here, we have n folds and E test emissivities. The emissivity that performs best on average is chosen.

fraction of the dataset equal to $(1 - 1/k)$ and $1/k$, respectively]. The emissivity model that features the minimum cost *on average* for all of the testing datasets is chosen as the correct one. Figure 8 illustrates the procedure.

B. Emissivity retrieval

The goal of the above procedure is to obtain an emissivity function $\hat{\epsilon}$ such that the temperature is accurately determined. $\hat{\epsilon}$ may differ from the true emissivity [e.g., a multiplicative constant in the emissivity does not change the predicted temperature in Eq. (5)] but still yield accurate temperature measurements. Once the temperature has been accurately determined, the *true* emissivity is retrieved with Eq. (1).

We use a simple polynomial decomposition of the emissivity on the domain of interest,

$$\hat{\epsilon}(\lambda) = \sum_{i=0}^{N_e} \hat{a}_i \lambda^i. \quad (34)$$

The procedure can be generalized to non-polynomial decompositions or polynomial bases that differ from the monomial one. Our initial values for the \hat{a}_i coefficients are

$$\hat{\mathbf{a}} = [0.5, 0, \dots, 0]. \quad (35)$$

The algorithm is not sensitive to the value of \hat{a}_0 . Figure 9 shows the flow-chart of the algorithm.

IV. RESULTS

In this section, we apply the above procedure on a variety of radiance measurements. For all of our tests, we use a value of $k = 10$ (i.e., the training and testing datasets represent roughly 90% and 10% of the dataset, respectively) to avoid simultaneously high bias and variance (Ref. 44, pp. 181–184).

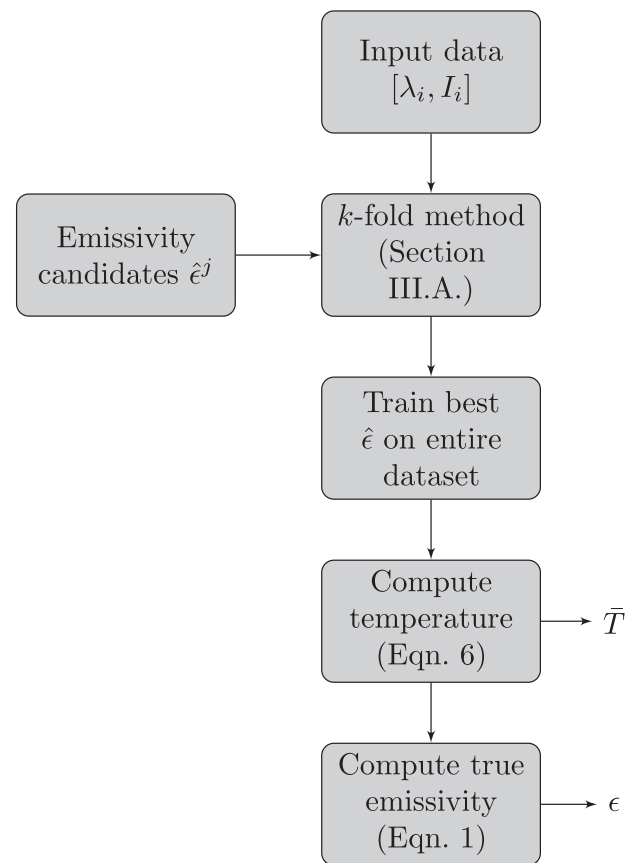


FIG. 9. Flow-chart of the algorithm.

For computational expediency, we choose to stop the training step of a single k -fold if the dispersion is below a given threshold α . During subsequent k -folds, the algorithm will still perform training on all proposed emissivity models unless one of them reaches the threshold first. If the distribution of the two-color temperature predictions is Cauchy-like, 50% of the predictions are within $[\bar{T}(1 - \alpha), \bar{T}(1 + \alpha)]$. The value of α was chosen based on a sensitivity analysis we present below. Polynomials for which training is not performed during a given k -fold are penalized (for *that* k -fold *only*) to favor lower-complexity ones.

A. Numerical experiments

We start with simulated radiance measurements perturbed with 10% Gaussian noise. The tests are designed to emulate the data obtained from a compact bench-top spectrometer equipped with a Czerny–Turner monochromator. The diffracted light is usually collected on a linear CCD array, where each pixel corresponds to a single, discrete wavelength. Typical CCD arrays have more than 3000 usable pixels. We consider that our hypothetical spectrometer provides radiance measurements at 3000 wavelengths in the visible range (400 nm–800 nm). We choose a moving average window of

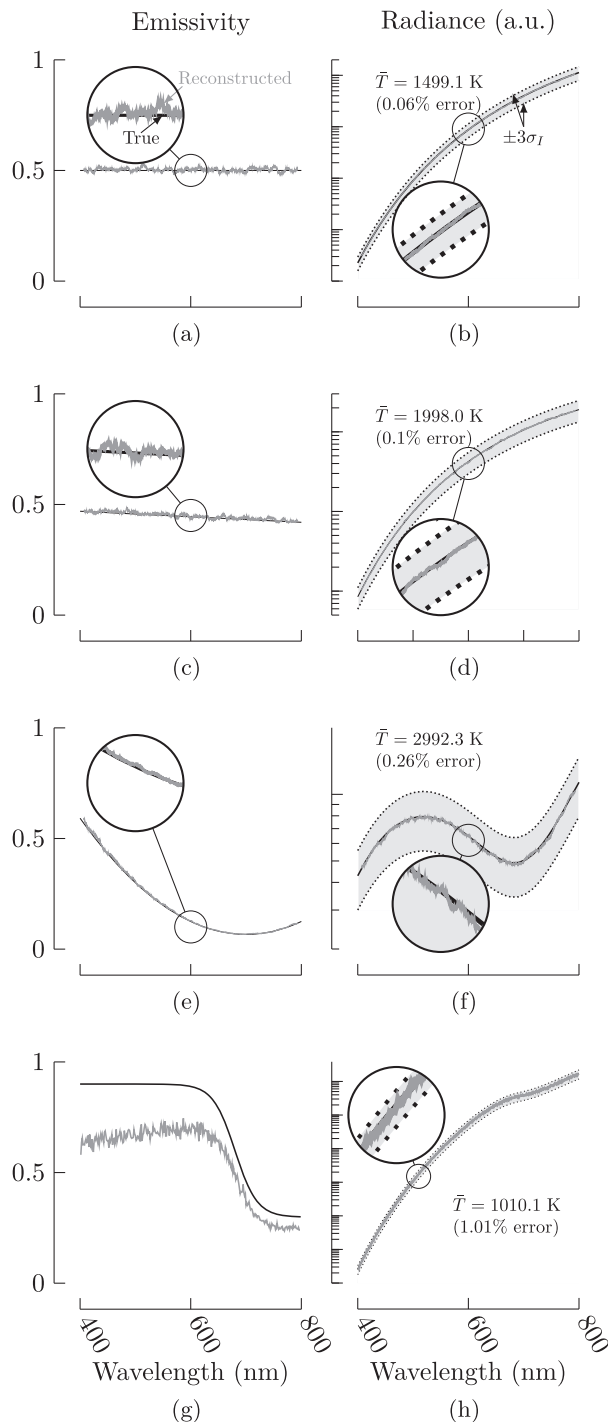


FIG. 10. Results of the algorithm for four numerical experiments, for the emissivity (left) and radiance (right). [(a) and (b)] Gray body case. [(c) and (d)] Linear emissivity. [(e) and (f)] Quadratic emissivity. [(g) and (h)] Logistic emissivity. Black and gray curves indicate the true and reconstructed values, respectively. The obtained temperature is indicated on the radiance graph along with the corresponding error. The confidence interval of the input “experimental” radiance ($\pm 3\sigma_I$) is shown (light gray).

size 51 to smooth the input radiance data and a threshold value of $\alpha = 5 \times 10^{-3}$.

1. Temperature and emissivity retrieval

We show in Fig. 10 the results of the procedure, as applied to four materials: a gray body of emissivity 0.5 at 1500 K, tungsten at 2000 K with linear emissivity (from Ref. 45), a material with an artificial second-order polynomial emissivity at 3000 K, and a material with an artificial emissivity that is similar to a logistic function at 1000 K (the case is similar to that shown in Ref. 29). The reconstructed emissivity is obtained from Eq. (1). The radiance is calculated from Eq. (2) with the reconstructed emissivity and the predicted temperature. In all cases, both the reconstructed emissivity and radiance closely match the true ones. The error in temperature is typically less than 1%, though in some cases the algorithm yields either an under- or over-fitted model for the emissivity. In those cases, the error incurred can be as high as 3%. However, the input

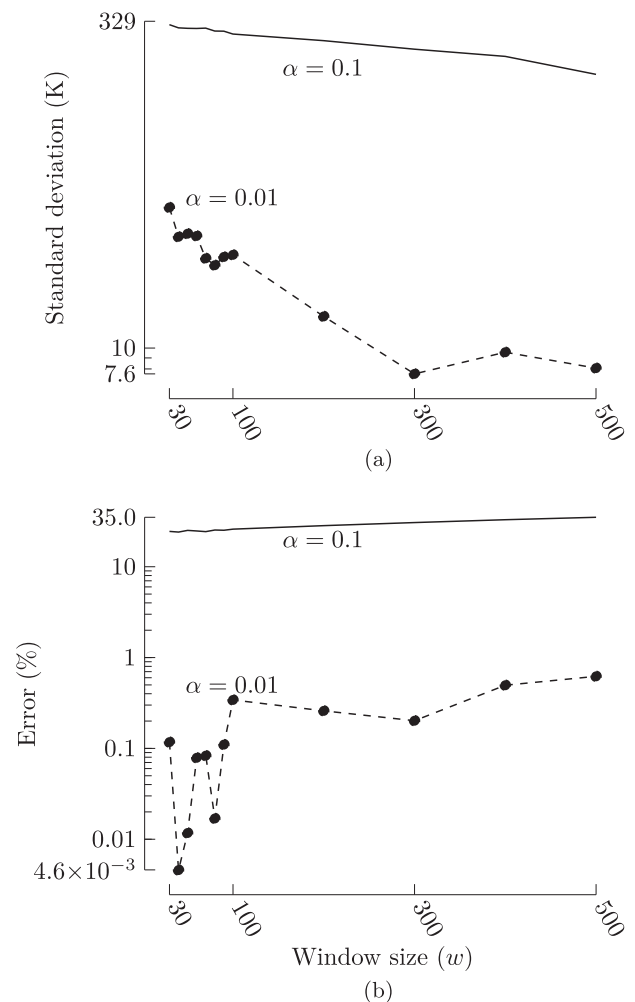


FIG. 11. Effect of thresholding parameter α and window size w on (a) standard deviation and (b) average error.

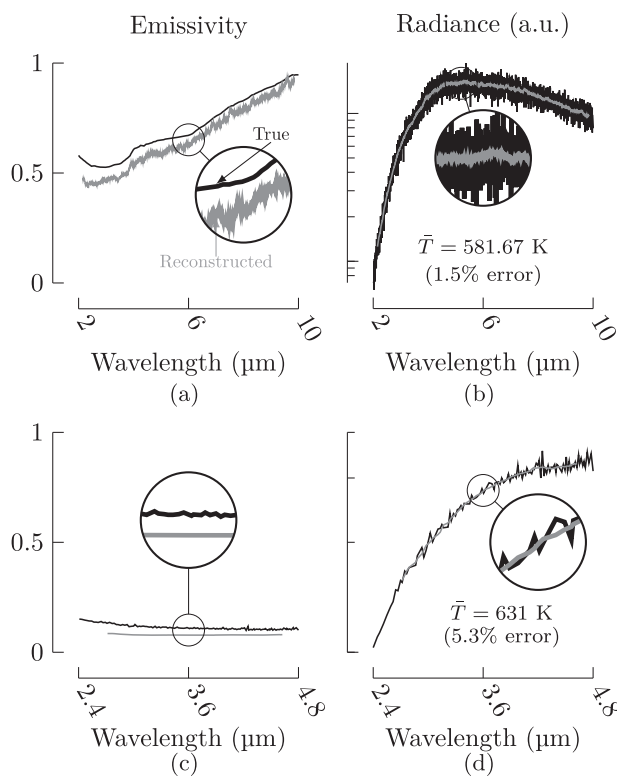


FIG. 12. Results of the algorithm as applied to experimental data. (a) Emissivity and (b) radiance for tantalum at 573 K. (c) Emissivity and (d) radiance for AL5083 aluminum at 600 K. The obtained temperatures are indicated on the radiance graph along with the corresponding error. Experimental data from Refs. 26 and 34 for AL5083 and tantalum, respectively.

data have 10% noise, which is much larger than the percentage error in temperature.

For the case of the logistic emissivity, we have sometimes observed reconstructed emissivities that are greater than 1, along with errors of up to 8%. We decreased the size of both the averaging window to 11 and the pixel bins to 29 from 51 and 50, respectively, to obtain the results shown in Fig. 10. Even with updated parameters, there are still instances where the procedure

cannot produce the expected results for this particular case. This possibly indicates that either the monomial basis or Nelder–Mead minimization method is inadequate, that the emissivity models chosen are inappropriate, or that the parameters of the method also require cross-validation.

2. Sensitivity analysis

We consider the case of the artificial quadratic emissivity at 1500 K and investigate the effect of thresholding (α) and window size (w) while keeping the input noise the same. We perform 1000 simulations and report in Fig. 11 the average error and standard deviation. For high values of α (>0.1), only the simplest emissivity models are considered (constant, linear) by the algorithm and the training is not performed on the quadratic emissivity. Because the emissivity model is then incorrect, the temperature error is large. For a critical value of α , training is performed for all of the models considered, and the error is minimum.

As suggested by Eq. (29), we also see that the standard deviation decreases with increasing window size for the digital filter. We note, however, that for large window sizes the error increases because the input data are overly smoothed.

B. Application to experimental data

We show in Fig. 12 the results of the procedure applied to experimental radiance and emissivity data retrieved from Refs. 26 and 34. The materials and temperature considered are the aluminum alloy AL5083 held at 600 K and tantalum held at a temperature of 573 K, respectively. For tantalum, we follow the same methodology as Ref. 34 and use the reported emissivity to generate the radiance curve. Table I shows the numerical values of the various parameters used for the two test cases.

We obtain good agreement for the radiance, emissivity [reconstructed with Eq. (1)], and temperature for both materials. For the aluminum alloy, the temperature error is 5.3%, a possible consequence of the small number of wavelengths available from the original data (108 unique wavelengths), which contribute to an ineffective filtering step and increased errors in the two-temperature ratios. The temperature error for the tantalum case is 1.5%, which is much smaller than the 10% noise imposed on the simulated radiance.

TABLE I. Numerical values of the parameters used for the test cases.

Parameter	Description	Aluminum test case	Tantalum test case
N	Number of unique wavelengths	108	3000
σ_I	Artificial measurement noise	N/A	0.1
α	Threshold		10^{-3}
w	Size of the filter window	11	51
N_e	Maximum polynomial order for the emissivity		4
k	Number of k -folds		10
N_{train}	Total number of wavelengths used for the training phase	79	2610
N_{test}	Total number of wavelengths used for the testing phase	9	290
L_{bin}	Size of the wavelength bin	3	50

V. CONCLUSION

We have presented a procedure to calculate the temperature of a surface with unknown emissivity, which, unlike previous procedures, is systematic and automated. For a given emissivity model, the temperature is calculated by averaging all possible combinations of a sufficiently large number of two-wavelength ratios. The emissivity model that minimizes the coefficient of dispersion is then chosen to calculate the temperature. Finally, the true emissivity is retrieved separately from the ratio of the measured radiance to that of a blackbody computed from the determined temperature. The choice of an emissivity model is automated through a cross-validation procedure that tests multiple emissivity candidates on randomly chosen subsets of the radiance measurements.

We have performed a statistical analysis to quantify the accuracy and precision of a procedure to compute the temperature of a surface with unknown emissivity from multiple radiance measurements that are subject to Gaussian noise. We successfully applied this method on both artificial and experimental data and illustrated the effect of the total number of wavelengths chosen, the wavelength range, and the chosen emissivity model on the procedure. We showed that, *for this particular procedure*, (i) increasing the number of wavelengths is always beneficial for both accuracy and precision, (ii) there exists an optimum wavelength range for which the precision is maximized, (iii) smoothing the input data with a moving average filter increases precision up to a point, and (iv) the interquartile dispersion is sensitive to the emissivity model (a low value of the dispersion indicates that the emissivity function chosen yields an accurate value of the temperature).

We note that a statistically significant number of two-wavelength ratios is required for the method to be applicable. A total number of wavelengths of 20 (190 ratios) or more are, therefore, required. We have also limited our analysis to polynomial representations (monomials) of the emissivity. In some cases, more complex test emissivity models or different polynomial representations may yield better temperature accuracy.

Other advantages of the methodology are as follows:

- The unknown coefficients of the emissivity function $\hat{\epsilon}$ do not have to be artificially bounded: an out-of-bound emissivity typically results in a high value for the cost function.
- The algorithm is not sensitive to the initial values of emissivity coefficients.
- The cross-validation ensures that a representation of the emissivity that returns the most accurate temperature is chosen.

The algorithm can be applied to challenging experimental or industrial settings in which both temperature and emissivity are functions of time (e.g., melting processes). The method can be easily extended to two-dimensional spectral measurements (e.g., hyperspectral imaging) and can be used to generate spatial temperature distributions, provided enough wavelengths are sampled.

ACKNOWLEDGMENTS

This work was supported by the Program in Plasma Science and Technology at Princeton University. The authors would like to

thank Sebastián Rojas Mata and Christopher Wordingham for their constructive comments.

APPENDIX: DERIVATIONS

1. Preliminary results

a. Expansion of functions of a random variable

Theorem A.1. *If X is a random variable that follows a normal distribution of mean μ_X and variance σ_X^2 [$X \sim \mathcal{N}(\mu_X, \sigma_X^2)$] and $f : X \mapsto f(X)$ is an arbitrary function, then the mean of $f(X)$ is given by*

$$\mathbb{E}[f(X)] = \sum_{n=0}^{N-1} \frac{\sigma_X^{2n} (2n-1)!!}{(2n)!} f^{(2n)}(\mu_X) + \mathcal{O}\left(\frac{\sigma_X^{2N} (2N-1)!!}{(2N)!} f^{(2N)}(\mu_X)\right). \quad (\text{A1})$$

The symbol $!!$ here denotes the double factorial,

$$(2N-1)!! = (2N-1)(2N-3)(2N-5)\cdots.$$

Proof. The Taylor expansion of $f(X)$ around μ_X is given by

$$f(X) = \sum_{k=0}^{N-1} \frac{1}{k!} f^{(k)}(\mu_X) (X - \mu_X)^k + \mathcal{O}\left(\frac{1}{N!} f^{(N)}(\mu_X) (X - \mu_X)^N\right).$$

The expected value of the sum is the sum of expected values,

$$\mathbb{E}[f(X)] = \sum_{k=0}^{N-1} \frac{1}{k!} f^{(k)}(\mu_X) \mathbb{E}[(X - \mu_X)^k] + \mathcal{O}\left(\frac{1}{N!} f^{(N)}(\mu_X) \mathbb{E}[(X - \mu_X)^N]\right).$$

Because $X \sim \mathcal{N}(\mu_X, \sigma_X^2)$, its odd moments are zero,

$$\forall k = 2n+1, n \in \mathbb{N}, \mathbb{E}[(X - \mu_X)^k] = 0,$$

and its even moments are given by

$$\forall k = 2n, n \in \mathbb{N}, \mathbb{E}[(X - \mu_X)^k] = \sigma_X^k (k-1)!!.$$

Replacing the k th order moment with the two previous formulas in the Taylor expansion for the expected value yields the theorem for the expected value of $f(X)$. \square

Theorem A.2. *If X is a random variable that follows a normal distribution of mean μ_X and variance σ_X^2 [$X \sim \mathcal{N}(\mu_X, \sigma_X^2)$] and $f : X \mapsto f(X)$ is an arbitrary function, then the variance of $f(X)$ is approximated by*

$$\text{Var}[f(X)] \approx \sigma_X^2 \left(f^{(1)}(\mu_X)\right)^2 + \frac{1}{2} \left(f^{(2)}(\mu_X)\right)^2 \sigma_X^4. \quad (\text{A2})$$

Proof. See Ref. 46. \square

Lemma 1. If X is a random variable that follows a normal distribution of non-zero mean μ_X and variance σ_X^2 and $\sigma_X/\mu_X \ll 1$, then $Y = \ln X$ can be approximated as a normal distribution of mean $\mu_Y = \ln \mu_X - \sigma_X^2/2$ and variance $\sigma_Y^2 = \sigma_X^2/\mu_X^2$. The truncation error for the mean is equal to $3/4(\sigma_X/\mu_X)^4$.

Lemma 2. If X is a random variable that follows a normal distribution of non-zero mean μ_X and variance σ_X^2 and $\sigma_X/\mu_X \ll 1$, then $Y = 1/X$ can be approximated as a normal distribution of mean $\mu_Y = 1/\mu_X(1 + \sigma_X^2/\mu_X^2 + 3\sigma_X^4/\mu_X^4 + 15\sigma_X^6/\mu_X^6)$ and variance $\sigma_Y^2 = \sigma_X^2/\mu_X^4$. The truncation error for the mean is equal to $105\sigma_X^8/\mu_X^9$.

Proof. This is a direct application of Theorems A.1 and A.2 where $f(X) = \ln X$ and $f(X) = 1/X$. \square

b. Validity of approximations

For $\ln X$ and $1/X$, the $2N$ th derivative that appears in the truncation error for the expected value [Eq. (A1)] is

$$\frac{\partial^{2N}(\ln X)}{\partial X^{2N}} = -\frac{(2N)!}{X^{2N}}$$

and

$$\frac{\partial^{2N}(1/X)}{\partial X^{2N}} = \frac{(2N)!}{X^{2N+1}}, \quad (\text{A3})$$

respectively. The truncation error, t_e , is, therefore,

$$t_e(\ln X) = \left(\frac{\sigma_X}{\mu_X}\right)^{2N} (2N-1)!!$$

and

$$t_e(1/X) = \left(\frac{\sigma_X}{\mu_X}\right)^{2N} \frac{(2N-1)!!}{\mu_X}, \quad (\text{A4})$$

respectively. From the Stirling approximation of the factorial, it can be shown that the double factorial that appears because of the moments of a normal distribution has the following asymptotic behavior:⁴⁷

$$(2N-1)!! \sim 2^N N^N \exp(-N) \sqrt{2}. \quad (\text{A5})$$

The truncation error of the expected value for both $\ln X$ and $1/X$, therefore, grows without bounds if more terms are added to the sequence (i.e., if $N \rightarrow +\infty$). We retain only the first few terms for the above approximations. The approximations are valid as long as $\sigma_X/\mu_X \ll 1$ and μ_X is non-zero.

2. Distribution of individual pair-wise temperatures

We show here that $\hat{T} \sim \mathcal{N}(\mu_{\hat{T}}, \sigma_{\hat{T}}^2)$, where both $\mu_{\hat{T}}$ and $\sigma_{\hat{T}}^2$ are given by Eq. (7). We assume that the radiance at each wavelength follows a normal distribution [$I \sim \mathcal{N}(\bar{I}, (\bar{I}\sigma_I)^2)$] with identical Gaussian noise.

Proof. We have that $\ln I \sim \mathcal{N}(\ln \bar{I} - \sigma_I^2/2, \sigma_I^2)$ from the results from Appendix 1 a. The difference of the two normal distributions $\ln I_i$ and $\ln I_j$ at two different wavelengths is also normally distributed. Its mean is equal to the difference of the means, and its variance is equal to the sum of the variances,

$$\ln I_i - \ln I_j \sim \mathcal{N}(\ln \bar{I}_i - \ln \bar{I}_j, 2\sigma_I^2).$$

The denominator of \hat{T} in Eq. (5) also follows a normal distribution because the wavelengths λ_i and λ_j and corresponding emissivities ϵ_i and ϵ_j do not follow a statistical distribution. Both quantities only affect the mean of the denominator of \hat{T} , μ_D ,

$$\begin{aligned} & \ln(I_i/I_j) - 5 \ln(\lambda_j/\lambda_i) - \ln(\epsilon_i/\epsilon_j) \\ & \sim \mathcal{N}(\ln(\bar{I}_i/\bar{I}_j) - 5 \ln(\lambda_j/\lambda_i) - \ln(\epsilon_i/\epsilon_j), 2\sigma_I^2) \\ & = \mathcal{N}(\mu_D, \sigma_D^2). \end{aligned}$$

We now apply the inverse function $1/X$ to the denominator of \hat{T} and find that it follows a normal distribution as per the results of Appendix 1 a. If we also multiply this distribution by the constants on the numerator of \hat{T} , we obtain

$$\begin{aligned} & C_2 \frac{1/\lambda_j - 1/\lambda_i}{\ln(I_i/I_j) - 5 \ln(\lambda_j/\lambda_i) - \ln(\epsilon_i/\epsilon_j)} \\ & \sim \mathcal{N}\left(C_2 \frac{1/\lambda_j - 1/\lambda_i}{\mu_D}, \left(C_2 \frac{1/\lambda_j - 1/\lambda_i}{\mu_D} \frac{\sigma_D}{\mu_D}\right)^2\right) \\ & = \mathcal{N}\left(T_{\text{eq}}, \left(T_{\text{eq}} \frac{\sigma_D}{\mu_D}\right)^2\right), \end{aligned}$$

where $T_{\text{eq}} = C_2 \frac{1/\lambda_j - 1/\lambda_i}{\mu_D}$. \square

DATA AVAILABILITY

The data and software that support the findings of this study are openly available at <https://doi.org/10.5281/zenodo.4021039>.

REFERENCES

- B. Müller, U. Renz, S. Hoppe, and F. Klocke, *J. Manuf. Sci. Eng.* **126**, 488 (2004).
- A. Hijazi, S. Sachidanandan, R. Singh, and V. Madhavan, *Meas. Sci. Technol.* **22**, 025106 (2011).
- D. P. DeWitt and R. E. Rondeau, *J. Thermophys.* **3**, 153 (1989).
- S. Liu, P. Farahmand, and R. Kovacevic, *Opt. Laser Technol.* **64**, 363 (2014).
- X. G. Sun, G. B. Yuan, J. M. Dai, and Z. X. Chu, *Int. J. Thermophys.* **26**, 1255 (2005).
- J. Estevadeordal, G. Wang, N. Nirmalan, A. Wang, S. P. Harper, and J. D. Rigney, *J. Turbomach.* **136**, 031004 (2014).
- D. Ketui, F. Chi, and G. Shan, *Measurement* **86**, 133 (2016).
- D. Ketui, F. Chi, and G. Shan, *Measurement* **92**, 218 (2016).
- M. V. Mekhregin, I. K. Meshkovskii, V. A. Tashkinov, V. I. Guryev, A. V. Sukhinets, and D. S. Smirnov, *Measurement* **139**, 355 (2019).
- A. G. McLean, J. W. Ahn, R. Maingi, T. K. Gray, and A. L. Roquemore, *Rev. Sci. Instrum.* **83**, 053706 (2012).
- E. Y. Choueiri, V. Chiravalle, G. Miller, and R. G. Jahn, in Proceedings of the 24th International Electric Propulsion Conference, 1995, IEPC-1995-067.
- J. E. Polk, C. M. Marrese-Reading, B. Thornber, L. Dang, L. K. Johnson, and I. Katz, *Rev. Sci. Instrum.* **78**, 093101 (2007).
- D. F. Simmons, C. M. Fortgang, and D. B. Holtkamp, *Rev. Sci. Instrum.* **76**, 044901 (2005).
- Y. A. Levendis, K. R. Estrada, and H. C. Hottel, *Rev. Sci. Instrum.* **63**, 3608 (1992).
- T. Fu, Z. Wang, and X. Cheng, *J. Heat Transfer* **132**, 051602 (2010).
- R. Khatami and Y. A. Levendis, *Combust. Flame* **158**, 1822 (2011).
- V. N. Bodrov, *High Temp.* **48**, 593 (2010).
- P. Hagqvist, F. Sikström, and A.-K. Christiansson, *Measurement* **46**, 871 (2013).
- P. Hagqvist, F. Sikström, A.-K. Christiansson, and B. Lennartson, *Meas. Sci. Technol.* **25**, 025011 (2014).

- ²⁰J. Xing, S. Cui, W. Qi, F. Zhang, X. Sun, and W. Sun, *Measurement* **67**, 92 (2015).
- ²¹J. Xing, R. S. Rana, and W. Gu, *Opt. Express* **24**, 19185 (2016).
- ²²M. Liang, B. Sun, X. Sun, and J. Xie, *Measurement* **95**, 239 (2017).
- ²³J. Liang, L. Dai, S. Chen, J. Xing, B. Peng, W. Gu, N. Jiang, W. Song, and J. Xing, *Opt. Express* **26**, 25706 (2018).
- ²⁴V. A. Kazakov and I. V. Senyuev, *Tr. Mai* **94** (2017) (in Russian).
- ²⁵C.-D. Wen, *Int. J. Heat Mass Transfer* **53**, 2035 (2010).
- ²⁶C.-D. Wen, *J. Mater. Eng. Perform.* **20**, 289 (2011).
- ²⁷C.-D. Wen and T.-Y. Chai, *Heat Mass Transfer* **47**, 847 (2011).
- ²⁸P. B. Coates, *Metrologia* **17**, 103 (1981).
- ²⁹A. Araújo and R. Silva, *Rev. Sci. Instrum.* **91**, 054901 (2020).
- ³⁰A. Araújo, *Meas. Sci. Technol.* **28**, 082002 (2017).
- ³¹T. Duvaut, *Infrared Phys. Technol.* **51**, 292 (2008).
- ³²M. A. Khan, C. Allemand, and T. W. Eagar, *Rev. Sci. Instrum.* **62**, 403 (1991).
- ³³G. R. Gathers, *Int. J. Thermophys.* **13**, 539 (1992).
- ³⁴T. Duvaut, D. Georgeault, and J. L. Beaudoin, *Infrared Phys. Technol.* **36**, 1089 (1995).
- ³⁵R. A. Felice, "Temperature determining device and process," U.S. patent 5772323 (June 30, 1998).
- ³⁶R. A. Felice, "Temperature determining device and process," U.S. patent 6,379,038 (April 30, 2002).
- ³⁷R. A. Felice, *AIP Conf. Proc.* **684**, 711 (2003).
- ³⁸H. Madura, M. Kastek, and T. Piątkowski, *Infrared Phys. Technol.* **51**, 1 (2007).
- ³⁹M. A. Khan, C. Allemand, and T. W. Eagar, *Rev. Sci. Instrum.* **62**, 392 (1991).
- ⁴⁰D. G. Bonett, *Comput. Stat. Data Anal.* **50**, 2953 (2006).
- ⁴¹F. Pedregosa, G. Varoquaux, A. Gramfort, V. Michel, B. Thirion, O. Grisel, M. Blondel, P. Prettenhofer, R. Weiss, V. Dubourg, J. Vanderplas, A. Passos, D. Cournapeau, M. Brucher, M. Perrot, and E. Duchesnay, *J. Mach. Learn. Res.* **12**, 2825 (2011).
- ⁴²J. A. Nelder and R. Mead, *Comput. J.* **7**, 308 (1965).
- ⁴³E. Jones, T. Oliphant, P. Peterson *et al.*, *SciPy: Open source scientific tools for Python*, 2001, accessed 10 September 2020.
- ⁴⁴G. James, D. Witten, T. Hastie, and R. Tibshirani, *An Introduction to Statistical Learning* (Springer, 2013).
- ⁴⁵D. R. Lide, *Handbook of Chemistry and Physics*, 77th ed. (CRC Press, 1997).
- ⁴⁶T. V. Anderson and C. A. Mattson, *J. Mech. Des.* **134**, 100911 (2012).
- ⁴⁷F. L. Bauer, *Math. Intell.* **29**, 10 (2007).